GEOPHYSICS, VOL. 71, NO. 3 (MAY-JUNE 2006); P. C37–C48, 11 FIGS., 2 TABLES.
10.1190/1.2194531

QVOA analysis: P-wave attenuation anisotropy for fracture characterization

Tatiana Chichinina[1], Vladimir Sabinin[1], and Gerardo Ronquillo-Jarillo[1]

ABSTRACT

This paper investigates Q-anisotropy for characterizing fractured reservoirs — specifically, the variation of the seismic quality factor Q versus offset and azimuth (QVOA). We derive an analytical expression for P-wave attenuation in a transversely isotropic medium with horizontal symmetry axis (HTI) and provide a method (QVOA) for estimating fracture direction from azimuthally varying Q in PP-wave reflection data. The QVOA formula is similar to Rüger's approximation for PP-wave reflection coefficients, the theoretical basis for amplitude variation with angle offset (AVOA) analysis. The technique for QVOA analysis is similar to azimuthal AVO analysis. We introduce two new seismic attributes: Q versus offset (QVO) gradient and intercept. QVO gradient inversion not only indicates fracture orientation but also characterizes Q-anisotropy. We relate the Q-anisotropy parameter ε_Q to fractured-medium parameters and invert the QVO gradient to estimate ε_Q. The attenuation parameter ε_Q and Thomsen-style anisotropy parameter $\varepsilon^{(V)}$ are found to be interdependent. The attenuation anisotropy magnitude strongly depends on the host rock's V_S/V_P parameter, whereas the dependence on fracture parameters is weak. This complicates the QVO gradient inversion for the fracture parameters. This result is independent of the attenuation mechanism. To illustrate the QVOA method in synthetic data, we use Hudson's first-order effective-medium model of a dissipative fractured reservoir with fluid flow between aligned cracks and random pores as a possible mechanism for P-wave attenuation.

INTRODUCTION

A preferential orientation of fracture networks makes fractured rocks azimuthally anisotropic. If these rocks are saturated with a fluid (e.g., oil, brine, or gas), then fluid flow between or within fractures (aligned cracks) and also from fractures to pores in the host rock may lead to azimuthally varying attenuation. The simplest model of such a medium is a dissipative transversely isotropic medium with a horizontal symmetry axis (HTI). Specifically, we assume Hudson's first-order effective-medium model (Hudson, 1981; Hudson et al., 1996).

Seismic properties such as azimuthally varying NMO velocity or amplitude variation with angle offset (AVOA) gradient can be used to determine fracture orientation and other parameters. Here, we study azimuthally varying attenuation and its potential application to fracture characterization. Since we analyze variations of Q-factor versus offset and azimuth, we call this method QVOA analysis (Chichinina et al., 2005) by analogy with azimuthal AVO. Studies by Crampin (1981), Hudson (1981), Thomsen (1995), and Chapman (2003) show that the more attenuated azimuth is perpendicular to the aligned cracks. If attenuation arises from intercrack flows, i.e., between parallel fractures that are aligned flow conduits, then attenuation anisotropy may be related to the anisotropy of horizontal permeability (Lynn, 2004). In the seismic frequency range, attenuation anisotropy has been observed and modeled in walkaround vertical seismic profilings (Horne and MacBeth, 1997; Maultzsch et al., 2003a) and surface seismic reflection data (Garrota, 1989; Lynn and Beckham, 1998; Clark et al., 2001).

Symmetry orientation can be extracted from azimuthal AVO by remembering that fracture-direction mapping as well as horizontal-earth-stress mapping are the objectives of azimuthal AVO analysis. What additional insights can we reach with QVOA analysis? First, it is important to know how Q-anisotropy causes changes in azimuthal AVO. Further, strong attenuation normal to the cracks may cancel the increase in reflectivity so that the symmetry orientations cannot be determined by azimuthal AVO methods (e.g., MacBeth, 1999; Maultzsch et al., 2003b). We believe that QVOA analysis can provide independent fracture-orientation indications that can be interpreted as the direction of maximum horizontal permeability (e.g., Lynn, 2004).

Generally, QVOA analysis uses Q-estimates extracted from

Manuscript received by the Editor December 1, 2004; revised manuscript received November 30, 2005; published online May 22, 2006.
[1]Instituto Mexicano del Petroleo, edificio 20, Eje Central Lazaro Cardenas, 152, c.p. 07730, Mexico City, DF, Mexico. E-mail: tchichin@imp.mx; vsabinin@yahoo.com; gronqui@imp.mx.

multiazimuthal 3D data by the spectral ratio method. Using the spectral ratio method, Q can be obtained for each trace of an azimuth-sectored common-midpoint (CMP) gather almost in the same manner that it is estimated from CMP gathers (Dasgupta and Clark, 1998; Hackert and Parra, 2004). Alternatively, the frequency-shift method can be used to derive the required Q-estimates. Its application to CMPs has been developed by Quan and Harris (1997) and Zhang and Ulrych (2002).

The objective of this paper is to provide a method (QVOA) for estimating fracture direction from azimuthally varying Q in PP-wave reflection data. We do this by developing an analytical expression for P-wave attenuation (the QVOA equation), which expresses almost linear dependence on squared sine of incidence angle. We illustrate the method with synthetic Q-data that was generated for Hudson's first-order effective-medium model of a dissipative fractured reservoir with fluid flow between aligned cracks and random pores (Hudson et al., 1996).

The paper is organized as follows. We first discuss the peculiarities of attenuation anisotropy as linked to velocity anisotropy — that is, Q-anisotropy of P-waves in an HTI medium, the effective-medium model of a fractured reservoir. Special emphasis is placed on the Q-anisotropy parameter ε_Q and its relation to the parameters of the fractured medium. We then present the formula for P-wave attenuation as a function of incidence angle and source-receiver azimuth and show that it resembles Rüger's approximation for P-wave reflection coefficients. This allows us to introduce new seismic attributes — QVO gradient and associated Q-intercept — which are analogous to AVO attributes. The azimuthal variation of Q versus offset (QVO) gradient enables us to find fracture-strike azimuth and other parameters of the fractured medium.

The maximum attenuation direction is in the symmetry-axis direction, unlike the maximum of the AVO gradient azimuthal parameter. In the latter case, the major semiaxis of the AVO ellipse can be oriented either parallel or perpendicular to fracture strike direction, depending on crack infill material, crack aspect ratio, and other factors (Hall and Kendall, 2000). Thus, azimuthal QVO analysis could resolve the ambiguity in fracture strike orientation. Moreover, Q-anisotropy may be more distinctive than reflection anisotropy, on which azimuthal AVO analysis is based.

THEORETICAL BACKGROUND

Here we review and develop the effective model of a dissipative fractured medium and introduce an anisotropy parameter of attenuation related to fractured-medium parameters.

HTI model of the dissipative fractured medium

To describe attenuation anisotropy, Carcione (2000) introduces a matrix $\mathbf{Q}$ of seismic quality factor Q for a homogeneous anisotropic viscoelastic medium. The elements Q_{ij} of the matrix $\mathbf{Q}$ are expressed in terms of components of the complex stiffness matrix $\widetilde{\mathbf{C}}, \widetilde{C}_{ij} = C_{ij}^R + iC_{ij}^I$ as

$$Q_{ij} = \frac{C_{ij}^R}{C_{ij}^I}, \tag{1}$$

where C_{ij}^R and C_{ij}^I denote real and imaginary parts and the tilde represents complex numbers.

The stiffness matrix $\mathbf{C}$ of the effective fractured HTI medium without attenuation (Schoenberg and Sayers, 1995),

$$\mathbf{C} = \begin{bmatrix} M(1-\Delta_N) & \lambda(1-\Delta_N) & \lambda(1-\Delta_N) & 0 & 0 & 0 \\ \lambda(1-\Delta_N) & M(1-\xi^2\Delta_N) & \lambda(1-\xi\Delta_N) & 0 & 0 & 0 \\ \lambda(1-\Delta_N) & \lambda(1-\xi\Delta_N) & M(1-\xi^2\Delta_N) & 0 & 0 & 0 \\ 0 & 0 & 0 & \mu & 0 & 0 \\ 0 & 0 & 0 & 0 & \mu(1-\Delta_T) & 0 \\ 0 & 0 & 0 & 0 & 0 & \mu(1-\Delta_T) \end{bmatrix}, \tag{2}$$

is expressed in terms of the dimensionless quantities Δ_N and Δ_T ($0 < \Delta_N < 1, 0 < \Delta_T < 1$), called normal and tangential weaknesses by Bakulin et al. (2000). Here, λ and μ are the host rock's Lamé constants, $M = \lambda + 2\mu$, $\xi = \lambda/M \equiv 1 - 2g$, and

$$g = \frac{\mu}{\lambda + 2\mu} = \left(\frac{V_S}{V_P}\right)^2, \tag{3}$$

where V_S and V_P are the host rock's S- and P-wave velocities and where g is defined in Bakulin et al. (2000).

The P-wave symmetry-axis velocity is

$$V^{\perp} = \sqrt{\frac{C_{11}}{\rho}} = V_P\sqrt{1-\Delta_N}, \tag{4}$$

and the isotropy-plane velocity is

$$V^{\parallel} = \sqrt{\frac{C_{33}}{\rho}} = V_P\sqrt{1-\Delta_N(1-2g)^2}. \tag{5}$$

From equations 4 and 5 it is clear that $V^{\perp} < V^{\parallel}$, i.e., the normal crack velocity is less than the in-crack velocity. (This result is true for $0 < \Delta_N < 1$ and $0 < g < 1/2$, which always hold.)

The dissipative HTI medium is described by the complex stiffness matrix $\widetilde{\mathbf{C}}$, obtained from the matrix $\mathbf{C}$ (equation 2) by substituting the real weaknesses Δ_N and Δ_T with complex weaknesses $\widetilde{\Delta}_N$ and $\widetilde{\Delta}_T$:

$$\Delta_N \rightarrow \widetilde{\Delta}_N = \Delta_N - i\Delta_N^I; \tag{6}$$

$$\Delta_T \rightarrow \widetilde{\Delta}_T = \Delta_T - i\Delta_T^I. \tag{7}$$

Then the phase velocities become complex, so that $\widetilde{V}^{\perp} = V_P\sqrt{1-\widetilde{\Delta}_N}$ and $\widetilde{V}^{\parallel} = V_P\sqrt{1-\widetilde{\Delta}_N(1-2g)^2}$.

Each element of $\mathbf{Q}$ from equation 1 can be expressed in terms of the complex weaknesses. For example, the P-wave symmetry-axis attenuation $1/Q^{\perp} \equiv 1/Q_{11}$ is

$$\frac{1}{Q^{\perp}} = \frac{\Delta_N^I}{1-\Delta_N}. \tag{8}$$

The isotropy-plane P-wave attenuation $1/Q^{\parallel} \equiv 1/Q_{33}$ is

$$\frac{1}{Q^{\parallel}} = \frac{\Delta_N^I(1-2g)^2}{1-\Delta_N(1-2g)^2}. \quad (9)$$

One can see from these expressions that $1/Q^{\perp} > 1/Q^{\parallel}$, i.e., the symmetry-axis attenuation is greater than the isotropy-plane attenuation.

The magnitude of the attenuation anisotropy is given by the ratio of $1/Q^{\perp}$ and $1/Q^{\parallel}$, or $Q^{\parallel}/Q^{\perp}$. From equations 4 and 5 for velocity and expressions 8 and 9 for attenuation, it follows that

$$\frac{Q^{\parallel}}{Q^{\perp}} = \frac{1}{\left[1-2\left(\frac{V_S}{V_P}\right)^2\right]^2}\left(\frac{V^{\parallel}}{V^{\perp}}\right)^2, \quad (10)$$

where $V_S/V_P \equiv \sqrt{g}$ (equation 3).

This expression shows that $Q^{\parallel}/Q^{\perp}$ is not dependent on Δ_N^I. The magnitude of the attenuation anisotropy is independent of the attenuation mechanism but strongly dependent on the host rock's V_S/V_P ratio and weakly dependent on the velocity ratio $V^{\parallel}/V^{\perp}$ (i.e., on the velocity anisotropy). In turn, $V^{\parallel}/V^{\perp}$ depends on the value of the normal weakness Δ_N, which involves fractured-medium parameters (crack density, crack aspect ratio, fluid bulk modulus, host rock shear modulus, and V_S/V_P; see the expression for Δ_N below).

Additionally, equation 10 shows that Q-anisotropy is stronger than velocity anisotropy:

$$\frac{Q^{\parallel}}{Q^{\perp}} > \frac{V^{\parallel}}{V^{\perp}}.$$

For example, for $V^{\parallel}/V^{\perp} = 1.2$ and $V_S/V_P = 0.5$, the symmetry-axis attenuation $1/Q^{\perp}$ is more than five times greater than the isotropy-plane attenuation $1/Q^{\parallel}$.

Fractured-medium parameters and normal weakness

Hudson's first-order theory for a fractured transversely isotropic effective medium (Hudson, 1981) can be presented in terms of real normal and tangential weaknesses Δ_N and Δ_T, as shown in the stiffness matrix (equation 2). The normal crack weakness Δ_N and the tangential weakness Δ_T, introduced for a nondissipative medium by Schoenberg and Douma (1988), are related to the fractured-medium parameters as follows:

$$\Delta_T = \frac{16e}{[3(3-2g)]}, \quad (11)$$

$$\Delta_N = \frac{4e}{3g(1-g)(1+K)}, \quad (12)$$

$$K = \frac{\kappa_f}{(\pi\mu a(1-g))}, \quad (13)$$

where e is crack density, μ is the host rock's shear modulus, and α is crack aspect ratio. The fluid can be gas, brine, or oil. The fluid bulk modulus κ_f depends on fluid P-wave velocities and densities (see Table 1).

As shown in Figure 1a, the normal weakness value Δ_N is greatest for the gas-filled crack model and increases with an increase in the crack aspect ratio α from $\alpha = 0.0001$ to $\alpha = 0.01$. For liquid-filled cracks (oil or brine filled), Δ_N is very small, and for very thin cracks ($\alpha < 0.01$) it can be considered equal to zero.

As shown by Bakulin et al. (2000), the small Δ_N value for liquid-saturated cracks results in the small absolute value of the P-wave anisotropy parameter $\varepsilon^{(V)}$ compared to the large $\varepsilon^{(V)}$ value for gas-filled cracks. Figures 1a and 1b show that the $\varepsilon^{(V)}$ dependence on the fracture parameters and V_S/V_P are similar to Δ_N dependence. We show below that $\varepsilon^{(V)}$ is proportional to Δ_N.

Q-anisotropy parameter ε_Q and velocity anisotropy parameter $\varepsilon^{(V)}$

Analogous with Thomsen's anisotropy parameter ε, where

$$\varepsilon = \frac{C_{11}-C_{33}}{2C_{33}}, \quad (14)$$

Carcione (2000) introduces the attenuation parameter ε_Q (denoted by ε^I):

$$\varepsilon_Q = \frac{Q_{11}-Q_{33}}{2Q_{33}}, \quad (15)$$

where, for an HTI medium, Q_{11} is the symmetry-axis quality factor $Q^{\perp}$ and Q_{33} is the isotropy-plane quality factor $Q^{\parallel}$.

We use the notation of Tsvankin (1997) and Rüger (1997) for the Thomsen-style anisotropy parameter ε for an HTI medium. That is, $\varepsilon^{(V)} = (C_{11}-C_{33})/(2C_{33})$, where C_{11} and C_{33} are the elements of the HTI stiffness matrix $\mathbf{C}$, given by equation 2. Note that $\varepsilon^{(V)}$ and ε_Q are negative because, in HTI media, $C_{11} < C_{33}$ and $Q_{11} < Q_{33}$.

Substituting the expressions for Q_{11} and Q_{33} (equations 8 and 9) into equation 15 yields a formula for the attenuation parameter ε_Q:

$$\varepsilon_Q = \frac{-2g(1-g)}{1-\Delta_N(1-2g)^2}. \quad (16)$$

Bakulin et al. (2000) derive the expression for the anisotropy parameter $\varepsilon^{(V)}$:

$$\varepsilon^{(V)} = \frac{-2g(1-g)\Delta_N}{1-\Delta_N(1-2g)^2}. \quad (17)$$

From equations 16 and 17,

Table 1. Fluid parameters.

Fluid	Fluid velocity V_f, (m/s)	Fluid density ρ_f, (kg/m^3)	Fluid bulk modulus κ_f, (Pa)
1) Gas	620	65	2.50×10^7
2) Brine	1710	1100	3.22×10^9
3) Oil	1250	800	1.25×10^9

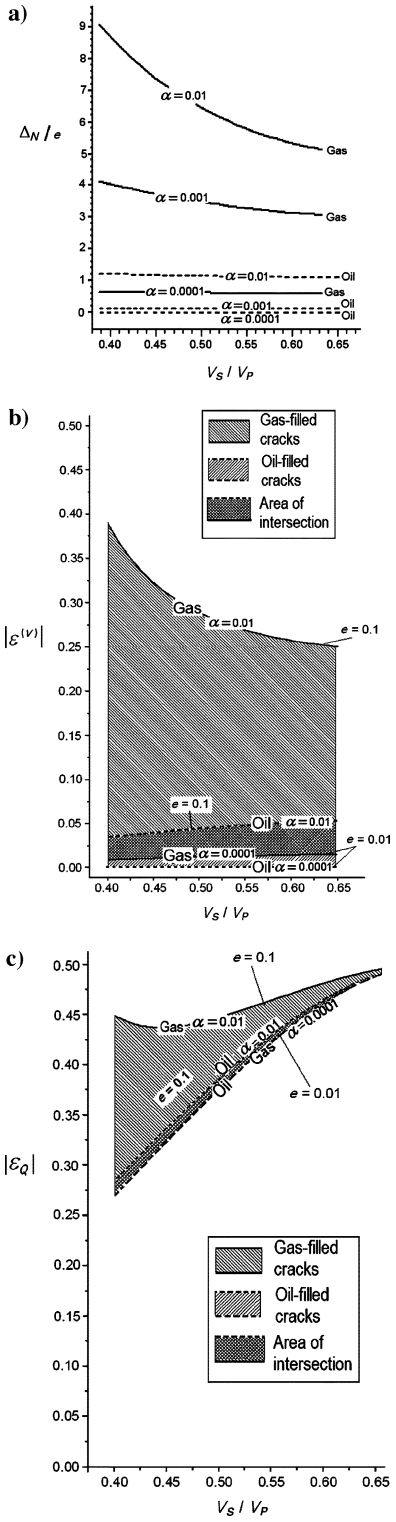

Figure 1. (a) The normal weakness Δ_N divided by crack density e and possible ranges of the parameters (b) $\varepsilon^{(V)}$, and (c) ε_Q versus the host rock's ratio V_S/V_P. (These are the absolute values of $\varepsilon^{(V)}$ and ε_Q.) In all figures, the dashed curve corresponds to the oil-filled crack model and the solid curve corresponds to the gas-filled crack model. The values of crack parameters (the crack aspect ratio α and the crack density e) are marked within and near the curves. Fluid parameters are given in Table 1, and the host rock's parameters are in Appendix A.

$$\varepsilon^{(V)} = \Delta_N \varepsilon_Q. \tag{18}$$

In Figure 1b and 1c, ranges of the anisotropy parameters $|\varepsilon^{(V)}|$ and $|\varepsilon_Q|$ are shown for oil-filled and gas-filled cracks as a function of the host-rock V_S/V_P-ratio. In Figure 1, the crack aspect ratio is constrained by $0.0001 \le \alpha \le 0.01$, and the crack density is constrained by $0.01 \le e \le 0.1$. The upper limit for $\varepsilon^{(V)}$ and ε_Q corresponds to $\alpha = 0.01$ and $e = 0.1$, and the lower limit corresponds to $\alpha = 0.0001$ and $e = 0.01$. The magnitude of Q-anisotropy, expressed by $|\varepsilon_Q|$, is much greater than the magnitude of the elastic anisotropy parameter $|\varepsilon^{(V)}|$ because $0 < \Delta_N < 1$. For example, if $V_S/V_P = 0.5$, the crack aspect ratio $\alpha = 0.001$, and the crack density $e = 0.1$, then for gas-filled cracks the normal weakness is $\Delta_N = 0.35$, the anisotropy parameters are $\varepsilon^{(V)} = -0.14$ and $\varepsilon_Q = -0.41$; therefore, $\varepsilon_Q \approx 2.9\varepsilon^{(V)}$. Since $\Delta_N(1 - 2g)^2 \ll 1$ in equation 17, an approximation for $\varepsilon^{(V)}$ is (Bakulin et al., 2000)

$$\varepsilon^{(V)} \approx -2g(1 - g)\Delta_N. \tag{19}$$

Thus, the anisotropy parameter $\varepsilon^{(V)}$ is approximately proportional to the normal weakness Δ_N, and its curve is similar to the curve for Δ_N (Figures 1a and 1b).

The inequality $\Delta_N(1 - 2g)^2 \ll 1$ also lets us write an approximation for ε_Q as

$$\varepsilon_Q \approx -2g(1 - g), \tag{20}$$

which is valid for thin, liquid-filled cracks ($\alpha \le 0.001$).

Equations 19 and 20 show that even for a very small anisotropy parameter $\varepsilon^{(V)}$ (as in the liquid-filled crack case, with $\Delta_N \approx 0$), the attenuation anisotropy parameter ε_Q can have a large absolute value. For example, $|\varepsilon_Q| = 3/8$ for $V_S/V_P = 0.5$. In this case, the symmetry-axis attenuation $1/Q^{\perp}$ is four times greater than the isotropy-plane attenuation $1/Q^{\parallel}$, i.e.,

$$\frac{Q^{\parallel}}{Q^{\perp}} = \frac{1}{2\varepsilon_Q + 1} = 4, \tag{21}$$

where $\varepsilon_Q = -3/8$, although there is no noticeable P-wave velocity anisotropy because $V^{\parallel}/V^{\perp} \approx 1$.

Note that the magnitude of attenuation anisotropy is independent of the imaginary part of the complex normal weakness Δ_N^I, whereas Δ_N^I defines the magnitude of P-wave attenuation $1/Q$ (equations 8 and 9). The value of Δ_N^I depends on the choice of the fluid-flow mechanism for attenuation (Hudson et al., 1996). Thus, the magnitude of Q-anisotropy does not depend on the type of attenuation mechanism.

Hudson's fluid-flow mechanisms as a cause of P-wave attenuation

In Hudson's models for a dissipative HTI medium, the fluid flow between (or within) microcracks causes P-wave attenuation. The weaknesses Δ_N and Δ_T become complex (equations 6 and 7) as a result of the complex frequency-dependent functions $\widetilde{M}(\omega)$ and $\widetilde{K}(\omega)$:

$$\widetilde{\Delta}_T = \frac{16e}{3(3 - 2g)(1 + \widetilde{M}(\omega))}, \tag{22}$$

$$\tilde{\Delta}_N = \frac{4e}{3g(1-g)(1+\tilde{K}(\omega))}. \quad (23)$$

Functions $\tilde{K}(\omega)$ and $\tilde{M}(\omega)$ differ for the three Hudson models. The three models are (1) fluid flow between interconnected cracks, (2) fluid flow from cracks into a background porous matrix (the equant porosity model), and (3) fluid flow within partially saturated cracks (Hudson et al., 1996; Pointer et al., 2000). In the seismic frequency range from 1–100 Hz, the function $\tilde{M}(\omega)$, which is responsible for predicting viscous energy dissipation, goes to zero for all three models (the result of Pointer et al., 2000). We assume that the tangential weakness $\tilde{\Delta}_T$ is real, but that the normal weakness $\tilde{\Delta}_N$ remains complex and its imaginary part dictates the magnitude of P-wave attenuation. The function $\tilde{K}(\omega)$ may be written as

$$\tilde{K}(\omega) = \frac{K}{1+\tilde{y}(\omega)}, \quad (24)$$

where K is defined by equation 13 and the complex frequency-dependent function $\tilde{y}(\omega)$ depends on the choice of the fluid-flow model. Maultzsch et al. (2003b) show that three gives negligibly small attenuation at seismic frequencies, whereas model one predicts large attenuation values in the seismic frequency range for models assuming gas-filled cracks and for large permeability values (>1000 mD). Consequently, we use model two for our numerical modeling, as given below (see also Appendix A).

P-WAVE ATTENUATION FOR ARBITRARY WAVE PROPAGATION IN HTI MEDIA

We have considered attenuation in the principal symmetry directions of an HTI medium (i.e., $1/Q^{\parallel}$ and $1/Q^{\perp}$) in equations 8 and 9. We now study azimuthally varying attenuation for an arbitrary direction of wavenormal.

The expression for P-wave phase velocity as a function of wavenormal angle φ with respect to the symmetry axis of a TI medium is given by the following expression (Schoenberg and Douma, 1988, p. 581):

$$V(\varphi)^2 = V_P^2(1 - \Delta_N[1 - 2g\sin^2\varphi]^2 - \Delta_T g \sin^2 2\varphi). \quad (25)$$

For a dissipative medium, the real normal weakness Δ_N in equation 25 should be replaced with the complex one, $\Delta_N - i\Delta_N^I$. Therefore, the phase velocity becomes complex:

$$\tilde{V}(\varphi)^2 = V_P^2(1 - (\Delta_N - i\Delta_N^I)[1 - 2g\sin^2\varphi]^2 - \Delta_T g \sin^2 2\varphi). \quad (26)$$

We assume that the tangential weakness Δ_T remains real according to the previous section.

To obtain the analogous expression for azimuthally varying attenuation, we use the following expression for attenuation (e.g., Carcione, 2000):

$$\frac{1}{Q} = \frac{\mathrm{Im}(\tilde{V}^2)}{\mathrm{Re}(\tilde{V}^2)}. \quad (27)$$

By extracting imaginary and real parts from squared complex phase velocity in equation 26, one can derive the following expressions:

$$\mathrm{Im}(\tilde{V}^2) = \Delta_N^I V_P^2[1 - 2g\sin^2\varphi]^2, \quad (28)$$

$$\mathrm{Re}(\tilde{V}^2) = V_P^2(1 - \Delta_N[1 - 2g\sin^2\varphi]^2 - \Delta_T g \sin^2 2\varphi) \equiv V(\varphi)^2. \quad (29)$$

By dividing one by the other, we get the expression for attenuation:

$$\frac{1}{Q} = \frac{\Delta_N^I[1 - 2g\sin^2\varphi]^2}{1 - \Delta_N[1 - 2g\sin^2\varphi]^2 - \Delta_T g \sin^2 2\varphi}. \quad (30)$$

Let θ denote the incidence angle measured with respect to the vertical z-axis, and let ϕ be the azimuth angle between the symmetry axis x and the source-receiver line. Then the unit wavenormal vector $\mathbf{n} = (\sin\theta\cos\phi, \sin\theta\sin\phi, \cos\theta)$ and the dot product of $\mathbf{n}$ by $\mathbf{x}$ is $(\mathbf{n}\cdot\mathbf{x}) = \cos\phi = \sin\theta\cos\phi$. By substituting $\sin^2\varphi$ with $1 - \sin^2\theta\cos^2\phi$ in equation 30, we find the attenuation as a function of θ and ϕ is

$$Q^{-1}(\phi,\theta) = \frac{\Delta_N^I[1 - 2g(1 - \sin^2\theta\cos^2\phi)]^2}{1 - \Delta_N[1 - 2g(1 - \sin^2\theta\cos^2\phi)]^2 - 4g\Delta_T\sin^2\theta\cos^2\phi(1 - \sin^2\theta\cos^2\phi)}. \quad (31)$$

The denominator of equation 31 can be written as $V^2(\theta,\phi)/V_P^2$, where, from equation 25,

$$V^2(\theta,\phi) = V_P^2(1 - \Delta_N[1 - 2g(1 - \sin^2\theta\cos^2\phi)]^2 - 4g\Delta_T\sin^2\theta\cos^2\phi(1 - \sin^2\theta\cos^2\phi)). \quad (32)$$

Then equation 31 can be rewritten as (Chichinina et al., 2004)

$$Q^{-1}(\phi,\theta) = \frac{\Delta_N^I[1 - 2g(1 - \sin^2\theta\cos^2\phi)]^2}{\frac{V^2(\theta,\phi)}{V_P^2}}. \quad (33)$$

Azimuthal variation of the attenuation calculated from QVOA equation 33 is shown in Figure 2. To calculate Q, the value of Δ_N^I is required. We have chosen Hudson's fluid-flow attenuation model 2, the equant porosity model (Hudson et al., 1996), to calculate the value of Δ_N^I in a seismic frequency range of $f = 30$ Hz (see Appendix A).

For all θ, the attenuation is maximum in the symmetry-axis azimuth $\phi = 0°$ (180°) and minimum in the isotropy plane $\phi = 90°$ (270°). The variation in the magnitude of attenuation is greatest for $\theta = 90°$, corresponding to horizontal propagation. In typical reflection data, incidence angles range from 0°–40°. The attenuation growth for the far offsets, e.g., $\theta = 40°$, is greatest, while for the

smaller incidence angles the magnitude of the attenuation variation decreases. Figure 2 shows that the magnitude of variation is small for the near-offset reflections ($\theta \leq 20°$); for zero offset, there is no variation.

THE PROBLEM OF ESTIMATING FRACTURE DIRECTION FROM AZIMUTHALLY VARYING Q

To detect azimuthal anisotropy by azimuthal amplitude analysis [AVOA, amplitude versus angle and azimuth (AVAZ), or azimuthal AVO (AVOZ)] and/or azimuthal NMO velocity analysis, one should use azimuth-sectored 3D data. QVOA analysis also requires azimuth-sectored CMP gathers. The QVOA method analyzes the Q-estimates from individual traces of azimuth-sectored CMP gathers. We assume that estimates of interval Q as a function of the angle of incidence have been computed by methods such as the spectral ratio method or the frequency-shift method. Here we use the synthetic Q-data to illustrate the prototype of the QVOA method.

The synthetic Q-data were generated from QVOA equation 33 for each of six mean azimuth-sector angles. These six source–receiver-line azimuths, $\phi = \phi_k$, $k = 1, 2, \ldots, 6$, are shown in Figure 3a. For now, we assume that the symmetry axis of the HTI layer does not coincide with the coordinate axis x and forms the angle ϕ_0 with it, as shown in Figure 3. The problem is to find ϕ_0 from azimuthally varying Q-data.

In the model, a P-wave reflects from the base of the fractured layer and is attenuated while passing through the layer (see Figure 3a). Our model is an idealized earth model with homogeneous, isotropic, and nonattenuative overburden. We assume a sufficiently thick (2–3 wavelengths) homogeneous fractured layer and frequency-independent reflection coefficients. For closely spaced reflectors, the effect of attenuation can be less pronounced and competes with other effects, such as interference from short-path multiplies or thin-bed influences (e.g., Hackert and Parra, 2004).

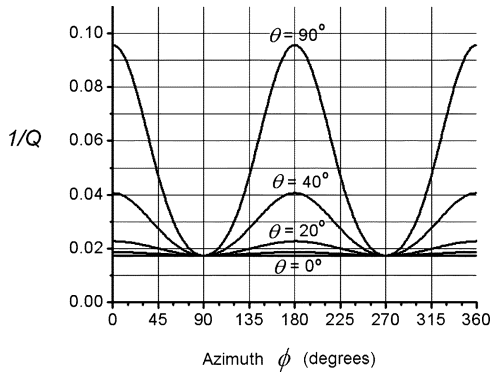

Figure 2. The curves graph the attenuation $1/Q$ versus the source–receiver-line azimuth ϕ as calculated from QVOA equation 33. The symmetry-axis azimuth is $\phi = 0°$ (180°). The curves correspond to different incidence angles θ as labeled. The fractured-medium parameters are $\alpha = 0.001$, $e = 0.1$, and $V_S/V_P = 0.5$. For this gas-filled-crack model (bulk modulus $\kappa_f = 2.50 \times 10^7$ Pa), the host rock's shear modulus $\mu = 1.47 \times 10^{10}$ Pa. This results in $\Delta_N = 0.35$. The parameter Δ_N^1 in the QVOA equation was calculated for Hudson's equant porosity model for the frequency $f = 30$ Hz, yielding $\Delta_N^1 = 0.064$. The input parameters and the equation for Δ_N^1 are given in Appendix A.

Synthetic Q-data as input for QVOA analysis

Figure 4 shows calculated values (from QVOA equation 33) of the inverse factor Q for the incidence angles θ from 0°–40° for six source–receiver-line azimuths ϕ_k ($k = 1, 2, \ldots, 6$): 0°, 36°, 72°, 108°, 144° and 180° (where the first and the last lines coincide: $\phi_1 = \phi_6$, i.e., 0° = 180°). As a model-input parameter, the symmetry-axis azimuth value is assumed to be $\phi_0 = 75°$.

In Figure 4, the azimuth $\phi = 72°$ is almost the symmetry-axis azimuth ϕ_0 ($\phi_0 = 75°$); that is why the attenuation growth is the greatest. For the azimuth angle $\phi = 144°$ or $\phi = 0°$ the attenuation growth is weak because these source-receiver lines are closer to the fracture-strike azimuth (the isotropy plane). On the other hand, Figure 4 shows that the far-offset attenuation (for $\theta = 40°$) is more than two times greater than the near offset (i.e., for $\theta = 0°$). The problem is to use these attenuation variations to resolve the fracture-direction estimation problem.

QVOA equation

The fan-shaped curve distribution in Figure 4 resembles the reflection-coefficient behavior in azimuthal AVO analysis. The solution of the problem may be the same, i.e., plot the attenuation curves versus $\sin^2\theta$ and analyze the line slopes.

Note that one should use the inverse square root values $Q^{-1/2}$ because the dependence $Q^{-1/2}$ is almost linear with respect to $\sin^2\theta$. Figure 5 shows $Q^{-1/2}$ as a function of $\sin^2\theta$, calculated from QVOA equation 33, which can be rewritten in the following form:

$$Q^{-1/2} = [A_0 + B^{\perp}\cos^2(\phi - \phi_0)\sin^2\theta]\frac{V_F}{V(\theta, \phi - \phi_0)}, \tag{34}$$

where

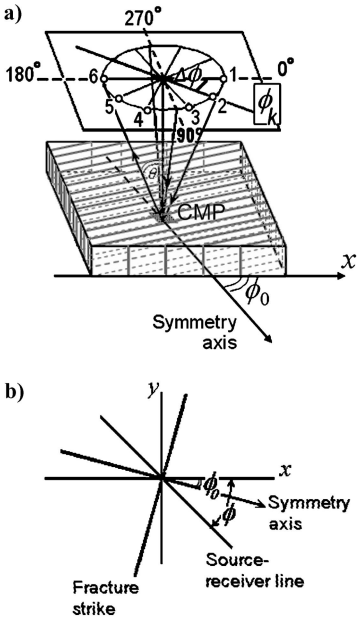

Figure 3. Six intersecting source-receiver lines (ϕ_k, $k = 1, 2, \ldots, 6$), corresponding to the CMP from the bottom of the HTI layer. (a) The x-axis coincides with the square-superbin side. (b) The symmetry axis forms an azimuth angle ϕ_0 with the x-axis, and angle ϕ is the source–receiver-line azimuth.

$$A_0 = \sqrt{\Delta_N^I}(1 - 2g) \tag{35}$$

and

$$B^{\perp} = \sqrt{\Delta_N^I}2g, \tag{36}$$

and where the symmetry-axis azimuth $\phi_0 = 75°$ and $\phi = \phi_k$ ($k = 1, 2, \ldots, 6$) are the source-receiver azimuths considered. Equation 34 may be considered a convenient form of QVOA equation 33.

The variation in V_P/V versus θ and ϕ in equation 34 does not significantly affect the variation of $Q^{-1/2}(\theta,\phi)$; therefore, this term can be considered constant, that is,

$$\frac{V_P}{V(\theta,\phi)} \rightarrow \frac{V_P}{\bar{V}_{\theta,\phi}} = c, \tag{37}$$

where $\bar{V}_{\theta,\phi}$ is the mean value of the velocity function $V(\theta,\phi)$, $0° \le \theta \le 90°$ and $0° \le \phi \le 360°$. In the symmetry-axis direction, the function $V(\theta,\phi)$ reaches its minimum value $V^{\perp} = V(90°,0°)$, which maximizes $V_P/V(\theta,\phi)$ and may be expressed from equation 4 as

$$\frac{V_P}{V^{\perp}} = (1 - \Delta_N)^{-1/2} \approx 1 + 0.5\Delta_N. \tag{38}$$

In the isotropy plane, $V_P/V(\theta,\phi)$ reaches its minimum value, which is, from equation 5,

$$\frac{V_P}{V^{\parallel}} = (1 - (1 - 2g)^2\Delta_N)^{-1/2} \approx 1 + 0.5(1 - 2g)^2\Delta_N, \tag{39}$$

where $0 < g < 1/2$ (if $0 < V_S/V_P < 0.7$) and $0 < \Delta_N < 1$. Then $V_P/V(\theta,\phi)$ lies in the interval $V_P/V^{\parallel} \le c \le V_P/V^{\perp}$, or

$$1 + 0.5(1 - 2g)^2\Delta_N \le c \le 1 + 0.5\Delta_N. \tag{40}$$

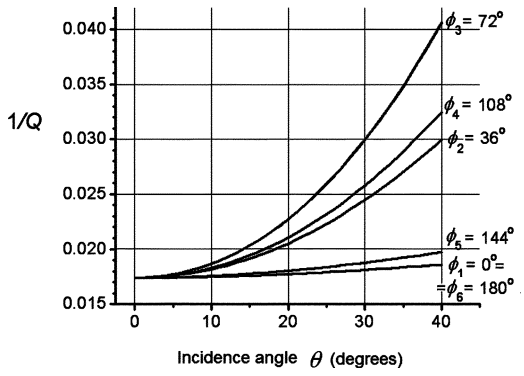

Figure 4. The attenuation $1/Q$ versus incidence angle θ, calculated for six source–receiver-line azimuths $\phi = \phi_k$ from QVOA equation 33, where $\phi_0 = 75°$. All model input parameters are the same as those used in Figure 2.

For thin, liquid-filled cracks with $\Delta_N \rightarrow 0$ (as shown above), $V_P/V(\theta,\phi)$ is approximately equal to unity. Then equation 34 can be rewritten as

$$Q^{-1/2} \approx A_0 + B^{\perp}\cos^2[\phi - \phi_0]\sin^2\theta \tag{41}$$

or

$$y = A_0 + Bx, \tag{42}$$

where $y \equiv Q^{-1/2}$, $x \equiv \sin^2\theta$, and $B = B^{\perp}\cos^2(\phi - \phi_0)$. Thus, QVOA equation 34 is approximately linear with respect to $\sin^2\theta$. Note that for gas-filled cracks, it is almost linear. In the latter case, the coefficients A_0 and B in equation 42 should be replaced with cA_0 and cB, respectively.

The line slope B is the QVO gradient, and the coefficient A_0 is the QVO intercept. The QVO gradient exhibits similar azimuthal angle dependence as the AVO gradient:

$$B(\phi) = 0{,}5(B^{\perp}\cos 2(\phi - \phi_0) + B^{\perp}). \tag{43}$$

Note that Rüger's linear approximation for the PP-reflection coefficient (Rüger, 1998) is valid only for incidence angles less than 10°, whereas the linear fit for the attenuation attribute $Q^{-1/2}$ is valid for angles of incidence from 0° to 40° because QVOA equation 34 is almost linear for all incidence angles up to $\theta = 90°$, as shown later.

QVOA analysis

For each individual azimuth-sectored CMP gather $\phi = \phi_k$ ($k = 1, 2, \ldots, 6$), QVO gradient B should be determined as shown in Figure 6. For the dependence $Q^{-1/2}(\sin^2\theta)$ extracted from an individual gather $\phi = \phi_k$, the linear least-squares-fit slope will provide QVO gradient value B_k and line intercept A_{0k}. In the same manner, the AVO gradient and the intercept are determined by azimuthal AVO (e.g., Mallik et al., 1998).

Figure 6 shows that the linear fit differs slightly from the data calculated from QVOA equation 34 because the equation is almost linear. To illustrate the procedure for estimating QVO gradient value, we choose the source-receiver azimuth with the greatest line slope, $\phi_3 = 72°$. The same procedure gives all pairs $(A_0,B)_k$, k

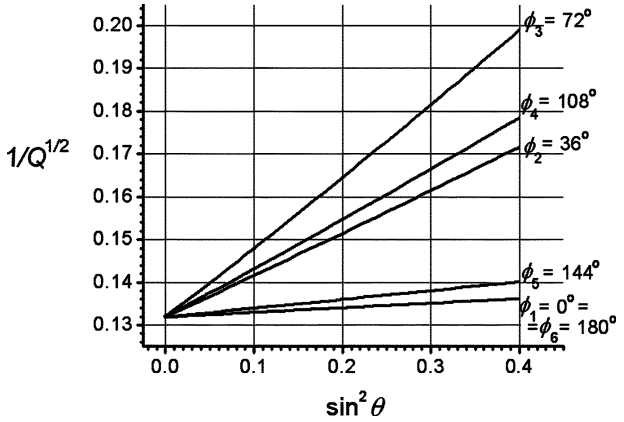

Figure 5. Same attenuation as in Figure 4, calculated for $Q^{-1/2}$ and plotted versus $\sin^2\theta$.

= 1, 2, … , 6. For each pair, the gradient B is divided by the corresponding intercept A_0 to produce six values B/A_0 of the normalized QVO gradient B,

$$B_k \equiv \left(\frac{B}{A_0}\right)_k, \quad k = 1, 2, \ldots, 6, \tag{44}$$

which are plotted versus azimuth $\phi = \phi_k$ in Figure 7.

According to equation 43, the $\cos 2\phi$ function should be fit to these six values B_k shown in Figure 7. For example, for gas-filled cracks the fit is $f(x) = 0.638 \cos 2(\phi - 75°) + 0.638$ (or $B^{\perp} = 0.638 \times 2 = 1.276$). For oil-filled cracks it is $f(x) = 0.548 \times \cos 2(\phi - 75°) + 0.548$ ($B^{\perp} = 1.096$). For both the oil-filled and gas-filled crack models the input parameters are given in Appendix A. The $\cos 2\phi$ fit maximum occurs at the symmetry-axis azimuth $\phi_0 = 75°$. The orthogonal direction, 165°, gives the fracture-strike orientation, which indicates the direction of maximum horizontal permeability or preferred fluid-flow direction.

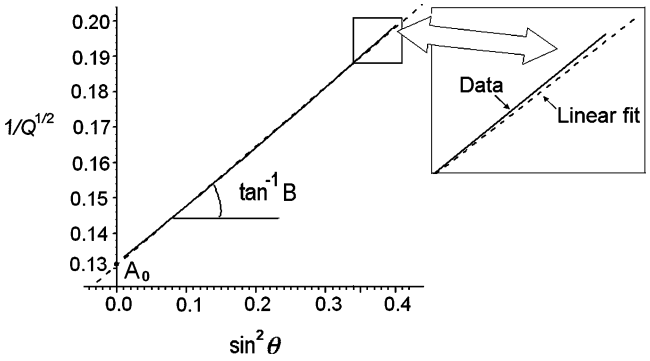

Figure 6. The attenuation attribute $Q^{-1/2}$ versus $\sin^2\theta$ calculated from QVOA equation 34 (solid line, marked as data) and its linear fit (dashed line). The linear-fit slope gives QVO gradient value B and line intercept A_0. This is one of six curves plotted in Figure 5 for a source-receiver azimuth $\phi_3 = 72°$. The enlarged curve fragment is shown to the right of the plot.

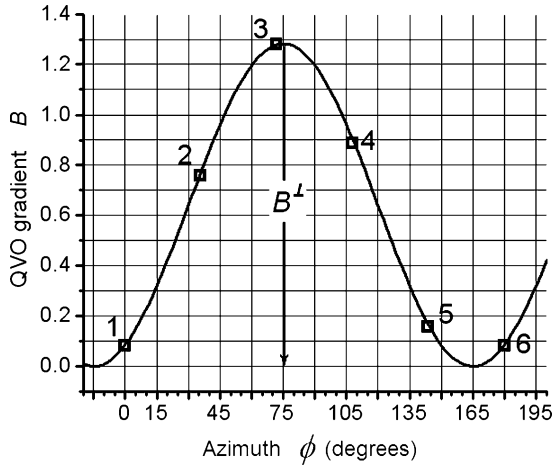

Figure 7. The normalized QVO gradient B (i.e., divided by the intercept $B = B/A_0$) versus azimuth ϕ. Six QVO gradient values $(B/A_0)_k$ for the gas-filled-crack model (marked by squares with numbers 1, 2, … , 6) and their $\cos 2\phi$ fit (solid line). The QVO gradient values for the six points correspond to the six functions $Q^{-1/2}$ plotted in Figure 5 (azimuths ϕ_1, ϕ_2, … , ϕ_6). The estimated fit-curve maximum value $B^{\perp}$ corresponds to the symmetry-axis direction $\phi_0 = 75°$.

PHYSICAL SENSE OF THE QVO GRADIENT

We have introduced a new seismic attribute, the QVO gradient (akin to NMO velocity or AVO gradient), which can be extracted from 3D wide-azimuth reflection data. We now consider other parameters that the QVO gradient can provide in addition to an estimate of fracture direction.

Quantitative estimation of Q-anisotropy

The physical sense of the QVO gradient value maximum $B^{\perp}$ in Figure 8 shows that the QVO gradient maximum value $B^{\perp}$ ($B^{\perp} \equiv B^{\perp}/A_0$) can be expressed as the relative difference between the attenuation factors $Q^{-1/2}$ in the principal symmetry directions,

$$B^{\perp} = \frac{(Q^{\perp})^{-1/2} - (Q^{\parallel})^{-1/2}}{(Q^{\parallel})^{-1/2}}, \tag{45}$$

where it is assumed from equation 41 that

$$(Q^{\parallel})^{-1/2} \approx A_0 \tag{46}$$

and

$$(Q^{\perp})^{-1/2} \approx A_0 + B^{\perp}. \tag{47}$$

Here, $(Q^{\parallel})^{-1/2}$ is the zero-offset $Q^{-1/2}$ value and $(Q^{\perp})^{-1/2}$ is the symmetry-axis $Q^{-1/2}$ value for $\theta = 90°$ and $\phi - \phi_0 = 0°$. Figure 8 shows the case of symmetry-axis-plane propagation, i.e., $\phi = \phi_0$.

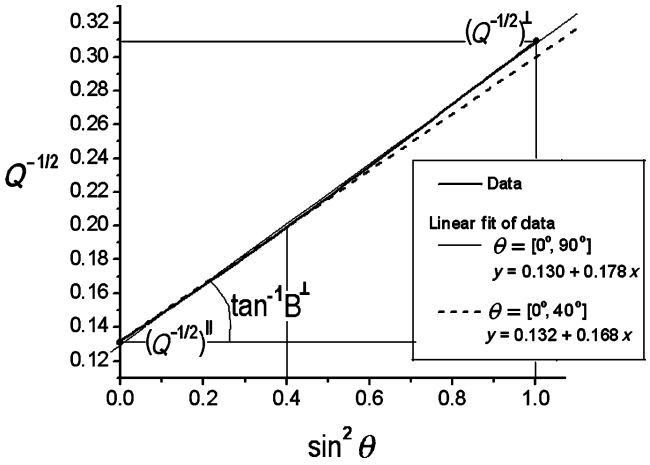

Figure 8. The parameter $Q^{-1/2}$ as a function of $\sin^2\theta$ (plotted by the thick, solid data line) calculated from QVOA equation 34 for the source–receiver-line azimuth $\phi = \phi_0$ (the symmetry-axis azimuth). The symmetry-axis attenuation $(Q^{\perp})^{-1/2}$ and the isotropy-plane attenuation $(Q^{\parallel})^{-1/2}$ are marked within the plot. The attributes $B^{\perp}$ and A_0 are estimated from the line slope of the linear fit for reflection data, i.e., in the θ interval [0°, 40°] (marked by vertical line $\sin^2\theta = 0.4$). The linear fit of Q in the interval of θ values [0°, 40°] (dashed line) differs from that in the interval [0°, 90°] (thin, solid line).

The exact expressions for $(Q^{\parallel})^{-1/2}$ and $(Q^{\perp})^{-1/2}$ in terms of A_0 and $B^{\perp}$ can be derived from QVOA equation 34 for $Q^{-1/2}(\theta,\phi - \phi_0)$, where $(Q^{\parallel})^{-1/2} \equiv Q^{-1/2}(0°,0°)$ and $(Q^{\perp})^{-1/2} \equiv Q^{-1/2}(90°, 0°)$:

$$(Q^{\parallel})^{-1/2} = A_0[1 - (1 - 2g)^2\Delta_N]^{-1/2}, \quad (48)$$

$$(Q^{\perp})^{-1/2} = (A_0 + B^{\perp})[1 - \Delta_N]^{-1/2}. \quad (49)$$

If $\Delta_N \ll 1$ and $(1 - 2g)^2\Delta_N \ll 1$, then the bracketed terms in equations 48 and 49 approach unity and the approximation of expression 45 for the attribute $B^{\perp}$ follows.

Thus, the QVO gradient $B^{\perp}$ can be interpreted as the Q-anisotropy indicator (equation 45). Quantitatively, the magnitude of Q-anisotropy can be expressed in terms of $B^{\perp}$, which can be converted to the parameter ε_Q as

$$\varepsilon_Q \approx 0.5\left(\frac{1}{[B^{\perp} + 1]^2} - 1\right). \quad (50)$$

Following equations 15, 48, and 49, the exact expression for ε_Q is

$$\varepsilon_Q = \frac{1}{2}\left(\frac{1 - \Delta_N}{[B^{\perp} + 1]^2(1 - (1 - 2g)^2\Delta_N)} - 1\right), \quad (51)$$

which reduces to the approximate equation 50 by assuming Δ_N goes to zero (e.g., the case of thin, liquid-filled cracks). This expression for ε_Q is more complicated than its approximation (equation 50); therefore, it cannot be applied to the inversion. Furthermore, it involves the unknown Δ_N.

For gas-filled cracks, using the estimated value $B^{\perp} = 1.276$, equation 50 provides the estimate $\varepsilon_Q = -0.4035$. Compared to the original input parameter, $\varepsilon_Q = -0.411$, the approximation gives 1.8% error. This error occurs not because of the linear-fit approximation inaccuracy but rather because of the error in estimating $B^{\perp}$ in the interval $\theta = [0°, 40°]$. The restriction of the incidence-angle interval is necessary because only this angle interval is usually available from reflection data, while the correct $B^{\perp}$ value should be estimated in the interval $[0°, 90°]$, as shown in Figure 8. Using the θ interval $[0°, 90°]$, the value $B^{\perp} = 1.37$ gives 100% accuracy in ε_Q estimation, or $\varepsilon_Q = -0.411$.

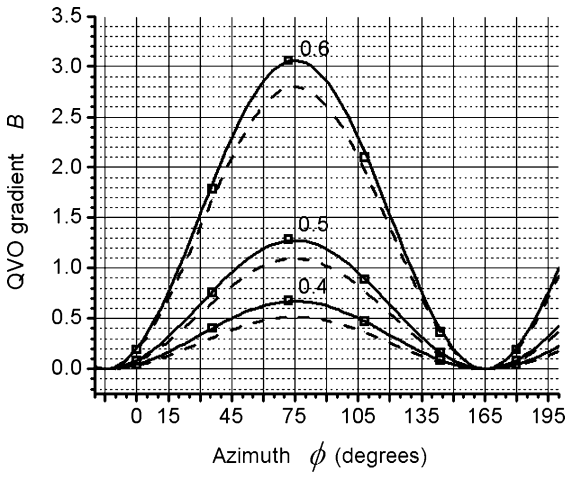

Figure 9. Azimuthal QVO gradient variation $B(\phi)$ estimated for gas-filled cracks (solid line with squares) and oil-filled cracks (dashed line) for $V_S/V_P = 0.4$, 0.5, and 0.6 (labeled in the plot). We show the normalized QVO gradient divided by the intercept A_0, $B(\phi) \equiv B(\phi)/A_0$.

Fractured-medium parameters and QVO gradient

We studied the behavior of the QVO gradient azimuthal variation for different host rock V_S/V_P ratios (Figure 9), for different crack-filling fluids (Figure 10a), and for different crack densities $e = 0.1$ and $e = 0.01$ (Figure 10b).

Figure 9 shows the growth of QVO gradient magnitude as the host rock's V_S/V_P ratio varies from 0.4 to 0.6. Comparing Figures 9, 10a, and 10b shows that the QVO gradient variation is more sensitive to the change of V_S/V_P ratio than to change in type of crack infill or crack density.

Figure 10a shows that the QVO gradient variation is smaller for liquid-filled cracks than for gas-filled cracks because Q-anisotropy

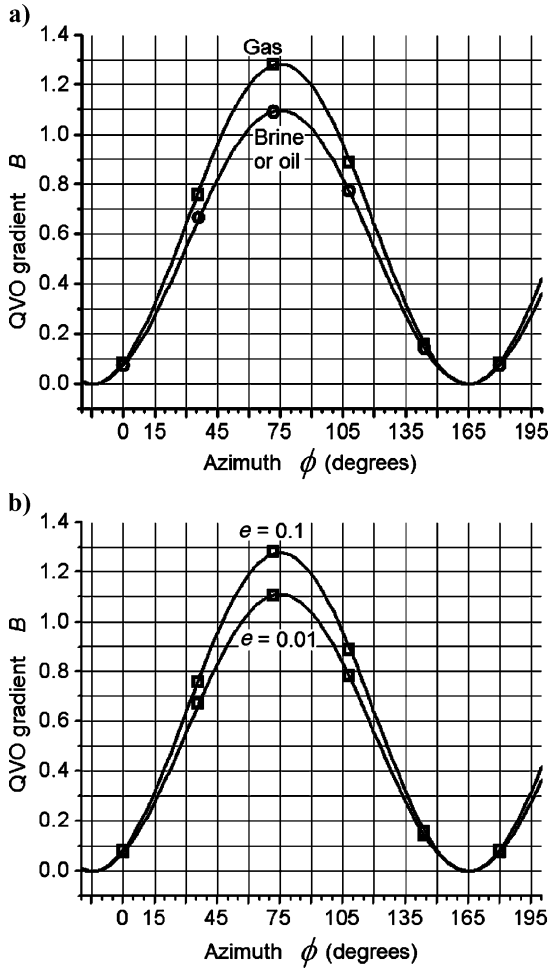

Figure 10. (a) Normalized QVO gradient B ($B(\phi) = B(\phi)/A_0$) for gas-filled cracks (squares) and liquid-filled cracks (circles) for the fixed crack density $e = 0.1$. (b) Same QVO gradient for gas-filled cracks for crack density $e = 0.1$ (upper curve) and $e = 0.01$ (lower curve). For both plots, $V_S/V_P = 0.5$ and the crack aspect ratio is $\alpha = 0.001$.

(or ε_Q) is smaller for liquid-filled cracks, as shown in Figure 1c. For the brine-filled crack model, the QVO gradient variation coincides with that for the oil-filled crack model.

Figure 10b shows the reduction in QVO gradient for gas-filled cracks attributable to a decrease in crack density e from 0.1 to 0.01; $B^{\perp} = 1.276$ goes to $B^{\perp} = 1.1$. This occurs because Q-anisotropy reduces as crack density decreases. (See ε_Q behavior in Figure 1c.)

Interestingly, Figures 10a and 10b look the same, and the reduction in the QVO gradient value $B^{\perp}$ is similar in both figures ($B^{\perp} = 1.276 \rightarrow B^{\perp} \approx 1.1$ in each case). This means the QVO gradient value is almost the same, $B^{\perp} \approx 1.1$, for the oil-filled crack model with $e = 0.1$ and the gas-filled crack model with $e = 0.01$. The similarity is explained by Figure 1a for Δ_N and by Figure 1c for ε_Q, from which one can infer that Δ_N and ε_Q values fall in the same range for these two cases (within the fixed crack aspect ratio value $\alpha = 0.001$ in both cases) and therefore the $B^{\perp}$ value is almost equal.

The QVO gradient inversion for the fracture parameters is complicated. Furthermore, the dependence on Δ_N is weak. However, the dependence of $B^{\perp}$ on the host rock's V_S/V_P parameter is very strong. Actually, from equations 34–36 and 45 the exact formula for $B^{\perp}$ is

$$B^{\perp} = \frac{1}{1-2g}\left[\frac{1-(1-2g)^2\Delta_N}{1-\Delta_N}\right]^{1/2} - 1. \qquad (52)$$

For thin, liquid-filled cracks, Δ_N goes to zero and the term in brackets goes to one in the last equation; therefore, $B^{\perp} \approx 2g/(1-2g)$, or

$$B^{\perp} \approx \frac{2\left(\frac{V_S}{V_P}\right)^2}{1-2\left(\frac{V_S}{V_P}\right)^2}. \qquad (53)$$

Then, an estimate of V_S/V_P is

$$\frac{V_S}{V_P} \approx \frac{1}{\sqrt{2\left(1+\frac{1}{B^{\perp}}\right)}}. \qquad (54)$$

For the example shown in Figure 10a, the liquid-filled crack model has $B^{\perp} = 1.096$. Equation 54 estimates $V_S/V_P = 0.51$ with a 2.3% relative error. The original model-input parameter is $V_S/V_P = 0.5$. For gas-filled cracks, the error is 5.8% ($B^{\perp} = 1.276 \rightarrow V_S/V_P = 0.53$) because Δ_N is greater ($\Delta_N = 0.35$) and approximation 53 does not fit very well.

Thus, the essential property of the QVO gradient is its strong dependence on the host-rock's V_S/V_P ratio. The magnitude of $B^{\perp}$ expresses the degree of Q-anisotropy and determines ε_Q. This is its main property, or its physical sense.

CONCLUSIONS

We have studied the behavior of P-wave attenuation as a function of offset (or angle of wave incidence) and azimuth and have shown that attenuation is strongest in the symmetry-axis plane (when perpendicular to the crack strike) and weakest in the isotropy plane (parallel to cracks). The magnitude of azimuthally varying attenuation increases along with incidence angle. We propose the QVOA method for estimating fracture direction from surface reflection data.

The relative difference in P-wave attenuation in directions parallel and perpendicular to fractures depends on fracture parameters and the host rock's V_S/V_P parameter. However, dependence on fracture parameters is weak. Consequently, fracture-parameter estimation is inaccurate from QVO gradient inversion, whereas the inversion for V_S/V_P is more stable, especially for thin, liquid-filled cracks. For liquid-filled cracks, Δ_N is very small and P-wave velocity anisotropy is weak. Therefore, the ratio $V_P/V(\theta,\phi)$, which is involved in the QVOA equation, is nearly equal to unity, and the QVO gradient is independent of fracture parameters and depends only on V_S/V_P.

The linear approximation is the most accurate for the liquid-saturated crack models. However, for gas-filled cracks the QVOA equation may be considered linear also, making the Q-data linear fit valid. The QVO gradient maximum $B^{\perp}$, extracted from the linear fit of Q-data, serves not only as the fracture strike-direction indicator but also as the Q-anisotropy indicator.

For the P-wave Q-anisotropy parameter, we suggest the parameter ε_Q. It is analogous to the anisotropy parameter $\varepsilon^{(V)}$ and corresponds to the conventional concepts of anisotropy, i.e., the fractional difference between the value of Q in horizontal and vertical directions of wave propagation. It is interesting that the attenuation parameter ε_Q, expressed in terms of fracture parameters, is equal to the velocity-anisotropy parameter $\varepsilon^{(V)}$ normalized by the normal weakness Δ_N, $0 < \Delta_N < 1$. From this we can conclude that Q-anisotropy is always greater than velocity anisotropy. The inversion of the QVO gradient maximum $B^{\perp}$ provides the ε_Q parameter estimate.

The attenuation-anisotropy magnitude strongly depends on the host rock's V_S/V_P parameter, whereas the dependence on fracture parameters is weak. This is a specific feature of P-wave Q- anisotropy, contrary to the velocity anisotropy. The result is entirely independent of Hudson attenuation mechanism. Nudson's equant porosity model was used only to calculate the attenuation value while generating the synthetic input data for QVOA analysis. Attenuation anisotropy also depends on the fractured medium's parameters. A change in crack parameters (fluid type, crack aspect ratio, crack density) changes the Δ_N value. In turn, the Δ_N change affects P-wave velocity and P-wave anisotropy. But its impact on P-wave attenuation anisotropy is small, and it is the smallest for liquid-filled cracks.

The algorithm of QVOA analysis is intended to work with estimates of attenuation attributes extracted from seismic reflection data. The Q-estimation problem itself is beyond the scope of this paper. The method is illustrated on synthetic Q-data. We also have investigated the accuracy of the approximation. In reality, attenuation estimation from seismic data is not easy; without an application to real data, the reliability of the method cannot be evaluated. We have only presented a prototype of a method. The next steps will be to develop the method, demonstrate the method on seismic data, and analyze the errors in the estimated parameters. The QVOA method may have an advantage over other approaches because it uses relative characteristics of attenuation and not the absolute ones known to be inaccurate.

ACKNOWLEDGMENTS

We express our sincere gratitude to the Mexican Petroleum Institute, where this study was fulfilled. We are grateful to Mark Chapman and anonymous reviewers for their helpful reviews. Also, we thank the editors for the corrections that considerably improved the paper clarity.

APPENDIX A

EQUANT POROSITY MODEL

In QVOA equation 33, the attenuation $1/Q$ is expressed through the imaginary part of the complex weakness $\tilde{\Delta}_N$, given by the general equation 23. For the equant-porosity model of Hudson et al. (1996), it is

$$\tilde{\Delta}_N = \frac{4e}{3g(1-g)(1+\tilde{K}(\omega))}, \tag{A-1}$$

where

$$\tilde{K}(\omega) = \frac{K}{1+\dfrac{3(1-i)J}{2c}} \tag{A-2}$$

$K = \kappa_f/(\pi\mu\alpha(1-g))$, $J = \sqrt{\phi_p K_r \kappa_f/(2\omega\eta_f)}$, and c is the crack half-thickness ($c = 10^{-4}$ m). The frequency-dependent function $J(\omega)$ includes new parameters such as the host rock's permeability K_r, the pore porosity ϕ_p, and the fluid viscosity η_f, given in Table A-1.

From equations A-1 and A-2, the imaginary part of $\tilde{\Delta}_N$, $\tilde{\Delta}_N = \Delta_N - i\Delta_N^I$, can be expressed as

$$\Delta_N^I = \frac{4e}{3g(1-g)} \frac{\dfrac{3JK}{2c}}{(1+3J/(2c)+K)^2 + (3J/(2c))^2}. \tag{A-3}$$

Figure A-1 plots isotropy-plane attenuation $1/Q^{\parallel}$, calculated from equation 9,

$$\frac{1}{Q^{\parallel}} = \frac{\Delta_N^I (1-2g)^2}{1-\Delta_N (1-2g)^2},$$

in which Δ_N^I is calculated from equation A-3 for the seismic-range frequency 30 Hz, $g = 1/4$ (or the host rock's parameter $V_S/V_P = \frac{1}{2}$), and model-input parameters in Table A-1.

The real normal weakness Δ_N is calculated from equations 12 and 13, that is,

$$\Delta_N = \frac{4e}{3g(1-g)\left[1+\dfrac{\kappa_f}{\pi\mu\alpha(1-g)}\right]}, \tag{A-4}$$

Table A-1. Model input parameters.

Crack model	η_f, Pa-s	K_r, (mD)	ϕ_p, (%)	$K_r \times \phi_p$, (mD)
Gas-filled	0.00002	1	1	0.01
Brine-filled	0.001	10	10	1
Oil-filled	0.02	100	10	10

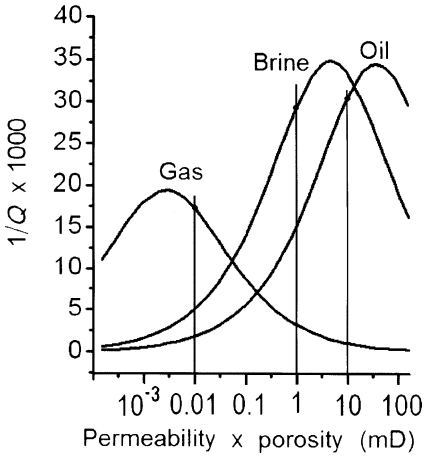

Figure A-1. The attenuation $1/Q$ versus permeability multiplied by porosity ($K_r \times \phi_p$) in the isotropy plane. The input crack parameters are $\alpha = c/a = 0.001$, $c = 10^{-4}$ m, and $e = 0.095$. Other parameters are given in Tables A-1 and 1. Vertical lines with the model numbers 1, 2, and 3 mark the values of the product $K_r \times \phi_p$, chosen for the model.

where the crack aspect ratio $\alpha = c/a = 0.001$, crack density $e = 0.095$, and the host rocks shear modulus $\mu = 1.47 \times 10^{10}$ Pa ($V_P = 4000$ m/s, $V_S = 2000$ m/s, and $\rho = 2550$ kg/m^3). The small crack-aspect ratio, $\alpha = 0.001$, is chosen because it gives a relatively large attenuation value and considerable P-wave anisotropy (e.g., Maultzsch et al., 2003b).

In Figure A-1, vertical lines 1–3 mark the values of the attenuation $1/Q$ and the values of the product (permeability $K_r \times$ porosity ϕ_p), corresponding to the gas-, brine-, and oil-filled crack models 1–3 (see Table A-1), which were chosen to calculate the synthetic Q-data to illustrate the QVOA method.

REFERENCES

Bakulin, A., V. Grechka, and I. Tsvankin, 2000, Estimation of fracture parameters from reflection seismic data — Part I: HTI model due to a single fracture set: Geophysics, **65**, 1788–1802.

Carcione, J. M., 2000, A model for seismic velocity and attenuation in petroleum source rocks: Geophysics, **65**, 1080–1092.

Chapman, M., 2003, Frequency-dependent anisotropy due to meso-scale fractures in the presence of equant porosity: Geophysical Prospecting, **51**, 369–379.

Chichinina, T., V. Sabinin, and G. Ronquillo-Jarillo, 2004, P-wave attenuation anisotropy in fracture characterization: Numerical modeling for reflection data: 74th Annual International Meeting, SEG, Expanded Abstracts, 143–146.

———, 2005, QVOA analysis as an instrument for fracture characterization: 75th Annual International Meeting, SEG, Expanded Abstracts, 127–130.

Clark, R. A., A. J. Carter, P. C. Nevill, and P. M. Benson, 2001, Attenuation measurements from surface seismic data: Azimuthal variation and time-lapse case studies: 63rd Meeting, EAEG, Extended Abstracts, paper L28.
Crampin, S., 1981, A review of wave motion in anisotropic and cracked elastic media: Wave Motion, **3**, 343–391.
Dasgupta, R., and R. A. Clark, 1998, Estimation of *Q* from surface seismic reflection data: Geophysics, **63**, 2120–2128.
Garrota, R., 1989, Detection of azimuthal anisotropy: 57th Annual International Meeting, SEG, Expanded Abstracts, 861–863.
Hackert, C. L., and J. O. Parra, 2004, Improving *Q* estimates from seismic reflection data using well-log-based localized spectral correction: Geophysics, **69**, 1521–1529.
Hall, S. A., and J.-M. Kendall, 2000, Constraining the interpretation of AVOA for fracture characterization: 9th International Workshop on Seismic Anisotropy (9IWSA), Anisotropy 2000, SEG, Proceedings, 1–38.
Horne, S., and C. MacBeth, 1997, AVA observations in walkaround VSPs: 67th Annual International Meeting, SEG, Expanded Abstracts, 290–293.
Hudson, J. A., 1981, Wave speeds and attenuation of elastic waves in material containing cracks: Geophysical Journal of the Royal Astronomical Society, **64**, 133–150.
Hudson, J. A., E. Liu, and S. Crampin, 1996, The mechanical properties of materials with interconnected cracks and pores: Geophysical Journal International, **124**, 105–112.
Lynn, H., 2004, The winds of change: Anisotropic rocks — Their preferred direction of fluid flow and their associated seismic signatures, part 1: The Leading Edge, **23**, 1156–1162.
Lynn, H., and W. Beckham, 1998, P-wave azimuthal variations in attenuation, amplitude and velocity in 3D field data: Implications for mapping horizontal permeability anisotropy: 68th Annual International Meeting, SEG, Expanded Abstracts, 193–196.
MacBeth, C., 1999, Azimuthal variation in P-wave signatures due to fluid flow: Geophysics, **64**, 1181–1192.
Mallik, S., K. L. Craft, L. J. Meister, and R. E. Chambers, 1998, Determination of the principal directions of azimuthal anisotropy from P-wave seismic data: Geophysics, **63**, 692–706.
Maultzsch, S., M. Chapman, E. Liu, and X. Y. Li, 2003a, Modeling frequency-dependent seismic anisotropy in fluid-saturated rock with aligned fractures: Implication of fracture size estimation from anisotropic measurements: Geophysical Prospecting, **51**, 381–392.
Maultzsch, S., S. Horne, S. Archer, and H. Burkhardt, 2003b, Effects of an anisotropic overburden on azimuthal amplitude analysis in horizontal transverse isotropic media: Geophysical Prospecting, **51**, 61–74.
Pointer, T., E. Liu, and J. A. Hudson, 2000, Seismic wave propagation in cracked porous media: Geophysical Journal International, **142**, 199–231.
Quan, Y., and J. M. Harris, 1997, Seismic attenuation tomography using the frequency shift method: Geophysics, **62**, 895–905.
Rüger, A., 1998, Variation of P-wave reflectivity with offset and azimuth in anisotropic media: Geophysics, **63**, 935–947.
Schoenberg, M., and J. Douma, 1988, Elastic wave propagation in media with parallel fractures and aligned cracks: Geophysical Prospecting, **36**, 571–590.
Schoenberg, M., and C. M. Sayers, 1995, Seismic anisotropy of fractured rock: Geophysics, **60**, 204–211.
Thomsen, L., 1995, Elastic anisotropy due to aligned cracks in porous rock: Geophysical Prospecting, **43**, 805–829.
Tsvankin, I., 1997, Reflection moveout and parameter estimation for horizontal transverse isotropy: Geophysics, **62**, 614–629.
Zhang, C., and T. Ulrych, 2002, Estimation of quality factors from CMP records: Geophysics, **67**, 1542–1547.